Tracking the ultraviolet-induced photochemistry of thiophenone during and after the ultrafast ring opening

Shashank Pathak¹⁺, Lea M. Ibele²⁺, Rebecca Boll³, Carlo Callegari⁴, Alexander Demidovich⁴, Benjamin Erk⁵, Raimund Feifel⁶, Ruaridh Forbes⁷, Michele Di Fraia⁴, Luca Giannessi^{4,8}, Christopher S. Hansen⁹, David M.P. Holland¹⁰, Rebecca A. Ingle¹¹, Robert Mason¹², Oksana Plekan⁴, Kevin C. Prince^{4,13}, Arnaud Rouzée¹⁴, Richard J. Squibb⁶, Jan Tross¹, Michael N.R. Ashfold^{15*}, Basile F.E. Curchod^{2*}, and Daniel Rolles^{1*}

*both authors have contributed equally *corresponding authors

¹J.R. Macdonald Laboratory, Department of Physics, Kansas State University, Manhattan, KS, USA

²Department of Chemistry, Durham University, Durham DH1 3LE, UK

³European XFEL, 22869 Schenefeld, Germany

⁴Elettra - Sincrotrone Trieste S.C.p.A., 34149 Basovizza, Trieste, Italy

⁵Deutsches Elektronen-Synchrotron, 22607 Hamburg, Germany

⁶Department of Physics, University of Gothenburg, Gothenburg, Sweden

⁷Stanford PULSE Institute, SLAC National Accelerator Laboratory, Menlo Park, CA 94025, USA

⁸Istituto Nazionale di Fisica Nucleare, Laboratori Nazionali di Frascati, 00044 Frascati (Rome),

Italy

School of Chemistry, University of New South Wales, Sydney NSW 2052, Australia
 Daresbury Laboratory, Daresbury, Warrington, Cheshire WA4 4AD, UK
 Department of Chemistry, University College London, London, WC1H 0AJ, UK
 Department of Chemistry, University of Oxford, Oxford, OX1 3TA, UK
 Centre for Translational Atomaterials, Swinburne University of Technology, Melbourne, Australia

¹⁴Max-Born-Institut, 12489 Berlin, Germany ¹⁵School of Chemistry, University of Bristol, BS8 1TS, UK

Abstract

Photo-induced isomerization reactions lie at the heart of many processes in nature. The mechanisms of such reactions are determined by a delicate interplay of coupled electronic and nuclear dynamics unfolding on the femtosecond scale, followed by the slower redistribution of energy into different vibrational degrees of freedom. Here we apply time-resolved photoelectron spectroscopy with a seeded extreme ultraviolet free-electron laser to trace the ultrafast ring opening of gas-phase thiophenone molecules following ultraviolet photoexcitation. When combined with *ab initio* electronic structure and molecular dynamics calculations of the excited- and ground-state molecules, the results provide insights into both electronic and nuclear dynamics of this fundamental class of reactions. The initial ring opening and non-adiabatic coupling to the electronic ground state is shown to be driven by ballistic S–C bond extension and to be complete within 350 femtoseconds. Theory and experiment also allow visualization of the rich ground-state dynamics – involving formation of, and interconversion between, ring-opened isomers and the cyclic structure, and fragmentation over much longer timescales.

Introduction

Recent advances in time-resolved experimental techniques and in computational methods for treating (coupled) electronic and nuclear dynamics are revolutionizing the field of ultrafast photochemistry, enabling direct probing of evolving molecular structures with unprecedented structural and temporal resolution¹⁻⁸. Such studies provide the ultimate test of our knowledge and understanding of light-initiated chemistry. Photo-induced ring-opening/closing reactions play a crucial role in many key processes in nature, *e.g.*, in the synthesis of natural products (such as previtamin D₃ by sunlight), and are currently attracting interest as molecular and biomolecular switches for photo-controlled switching of enzyme activity, optical data storage, modulating energy and electron transfer processes^{9,10} and in potential medical applications¹¹. Ring-opening reactions featured prominently in the development of the Woodward-Hoffmann rules that help rationalize the mechanisms and outcomes of pericyclic reactions. It is now recognized that photo-induced isomerization (including ring-opening) reactions are governed by strong non-adiabatic coupling between multiple electronic states of the molecule via conical intersections, which represent a breakdown of the Born-Oppenheimer approximation^{5,12}.

The photo-induced ring opening of the polyene 1,3-cyclohexadiene¹³ is widely employed as a model system for benchmarking and validating ultrafast methods, *e.g.* by ultrafast X-ray^{1,7,8} and electron⁶ diffraction, by femtosecond transient X-ray absorption⁴ and fragmentation¹⁴, and by time-resolved photoelectron spectroscopy (TRPES)¹⁵⁻¹⁶. However, few other photo-induced ring-opening reactions have been probed so thoroughly and, of these, even fewer have provided a comprehensive picture of the reaction dynamics on both the excited and ground (S₀) state potential energy surfaces (PESs).

Here we report a combined theoretical and experimental study of the ultraviolet (UV) photoinduced ring opening of a prototypical heterocyclic molecule, 2(5H)-thiophenone (C₄H₄OS, henceforth thiophenone; see Fig. 1). Heterocyclic compounds are fundamental building blocks in the synthesis of many organic compounds. Studying these "single units" may help in validating the (necessarily more complex and less resolvable) photochemistry of ever larger molecules. The study is conducted in the gas phase (*i.e.* under collision-free conditions) and thus reveals information on the purely intramolecular relaxation pathways, without the solvation effects present in previous matrix isolation¹⁷ and liquid-phase¹⁸ studies of this system. Theory and experiment combine to afford detailed insights into both the mechanism and time scale of the initial ring-opening process, and the subsequent evolution of the vibrationally excited ground-state photoproducts.

The experimental study employs the extreme ultraviolet (XUV) radiation provided by the free-electron laser (FEL) FERMI¹⁹. TRPES^{20,21} is sensitive to both electronic and structural dynamics – which is essential for any full understanding of the coupled electronic and nuclear dynamics that govern most photo-induced reactions. TRPES also allows access to so-called 'dark' states that may not be amenable to study by transient absorption methods. XUV probe pulses (from an FEL or a high harmonic generation source) are sufficiently energetic to ionize molecules in the electronic ground state (S₀) – thereby overcoming a long-recognized shortcoming of TRPES studies that employed lower energy (UV) photons and were thus unable to reveal the ultimate structural dynamics following transfer from an electronically excited state to the ground state ^{16,22-26}. FERMI is a seeded FEL^{19,27}, in which an external laser is used to initiate the XUV generation, offering the advantages of (i) a narrower photon energy bandwidth, *i.e.* higher energy resolution, and higher stability compared to FELs based on self-amplified spontaneous emission (SASE), and (ii) higher pulse energies and photon fluxes as compared to monochromatized XUV sources based on high harmonic generation.

In the present experiment, gas-phase thiophenone molecules are excited to the optically bright S₂ electronic state by a UV pulse ($\lambda \approx 265$ nm). The excited molecules evolve through one or more conical intersections at progressively greater C-S bond separations en route back to the S₀-state PES, where they can adopt the original closed-ring or several possible open-ring geometries 18,28, some of which are sketched in Fig. 1. The evolving wavepacket and the formation of open- and closed-ring photoproducts are probed by ionizing the molecule with a time-delayed 19.24-eV (λ = 64.44 nm) XUV pulse. Time-dependent photoelectron time-of-flight spectra are recorded as a function of time delay (Δt) between the UV and FEL pulses using a magnetic-bottle spectrometer (see Methods and Supplementary Fig. 1). The FEL photon energy is deliberately chosen to be well above the first ionization potential (IP) of the ground state molecule (~9.7 eV)²⁹ but below the IP of the helium carrier gas, ensuring that the electronic character of the target molecule can be traced throughout the complete structural evolution with only minimum background signal from the carrier gas. The experimental results are complemented by high level ab initio electronic structure and molecular dynamics calculations of both excited- and ground-state molecules, which afford insight into the ultrafast electronic de-excitation that accompanies ring opening and the subsequent interconversion between different isomeric forms of the highly vibrationally excited ground-state photoproducts.

Results and Discussion

Experimental Results. The experiment measures electron time-of-flight spectra of thiophenone as a function of Δt , which are converted to electron kinetic energy spectra and then, by energy

conservation, into spectra of the valence binding energies (see Methods). Fig. 2(a) shows such spectra in the form of a two-dimensional (2-D) plot of electron yield as functions of binding energy (BE) and Δt . The dominant feature at BE ~9.7 eV is due to photoionization of the "cold" (*i.e.* non-excited) closed-ring S₀-state thiophenone molecule²⁹. This peak is depleted by ~20% for positive Δt , as shown in Fig. 2(b) (red circles), confirming excitation of ground-state molecules by the UV pulse. A fit to the delay-dependent yield of photoelectrons originating from S₀-state parent molecules yields an upper limit for the temporal instrument response function of $\sigma = 72 \pm 8$ fs. Fig. 2(a) reveals photoelectrons with BEs as low as ~5 eV at the shortest positive Δt . The prompt appearance and subsequent decay of this contribution is also emphasized in Fig. 2(b), which shows a Gaussian-shaped transient signal with $\sigma = 76 \pm 6$ fs (blue triangles). With increasing delay, the signal at BE ~5 eV fades and the peak intensity shifts toward higher BE. As Fig. 2(c) shows, the peak in the intensity vs Δt transient obtained by taking contiguous 0.6 eV-wide slices for BE \geq 5.3 eV shifts to progressively later Δt with increasing BE, and the transients gain an increasingly obvious tail.

The thiophenone cation has close-lying ground (D_0) and first excited (D_1) states at a vertical IP (IP_{vert}) of ~9.7 eV, and higher excited states at IP_{vert} values of 10.58 eV (D_2), 12.25 eV (D_3) and 14.1 eV (D_4)²⁹. Given the present pump photon energy of 4.67 eV, the signal appearing at a binding energy of ~5 eV at Δt ~0 is readily attributed to vertical ionization of photoexcited molecules in the S_2 state to the (unresolved) D_0 and D_1 states. Ionization to the latter is strongly disfavored due to selection rules, as discussed in Section 2.3 of the Supplementary Information. The evolution of the signal at BE ~5 eV, the peak shift towards higher BE at later Δt , and the more intense tail in the Δt traces for higher BE slices all reflect the complex evolution of the photo-prepared wavepacket, which the accompanying theory shows involves ultrafast depopulation of the S_2 state to yield "hot", *i.e.*, highly vibrationally excited, S_0 (henceforth $S_0^{\#}$) molecules (revealed by the teal green stripe in Fig. 2(a) at BE ~9 eV). Note that any photoelectrons arising from ionization of $S_0^{\#}$ molecules to excited D_n (n > 1) cation states are likely to appear at BE >10 eV (see extended spectrum in Supplementary Fig. 2), and thus do not affect the discussion that follows.

Calculations of decay pathways and excited-state dynamics. To interpret the dynamics revealed in the TRPES spectra, the lowest-lying PESs of thiophenone were computed and different critical points located using SA(4)-CASSCF(10/8) calculations, and their energies further refined using XMS(4)-CASPT2(10/8) (see Computational Details for more information). The Franck-Condon (FC) geometry corresponds to the equilibrium structure of the S₀-state of thiophenone, wherein the highest occupied molecular orbital (HOMO) is an out-of-plane π orbital largely localised on the S atom, henceforth labelled n(S). At our chosen pump photon energy, thiophenone is predominantly excited to its S₂ state. At the XMS(4)-CASPT2(10/8) level of theory, the S₀ \rightarrow S₂ transition has $n(S)/\pi^*$ character, a calculated transition energy of 4.67 eV and an appreciable oscillator strength (0.036) – reflecting the constructive overlap of the donating n(S) and accepting π^* orbitals. The S₀ \rightarrow S₁ transition (with a calculated energy of 4.20 eV), in contrast, has $n(O)/\pi^*$ character and is dark (the donating n(O) orbital lies in the plane of the ring and is thus orthogonal to the accepting orbital, see Section 2.1 in the Supplementary Information). Different minimum energy conical intersections (MECIs) were located between the S₂, S₁, and S₀ states of thiophenone, as shown in

Fig. 3(a). All of these MECIs indicate a ring opening in the excited electronic state (*i.e.* formation of a biradical), followed by geometrical relaxation – e.g. twisting of the CH₂–S moiety out of the molecular plane and bending of the C–C=O moiety (see also Section 2.2 in the Supplementary Information).

To determine the possible connections between these critical structures and the relaxation pathways of thiophenone following UV photoexcitation, linear interpolations in internal coordinates (LIICs) were performed using XMS(4)-CASPT2(10/8) (see Computational Details). Starting from the FC geometry, the LIICs smoothly connect the different critical points and confirm that photoexcited thiophenone (S2) molecules can relax efficiently towards the S0 state via the S₂/S₁ and S₁/S₀ seams of intersection in the C-S bond extension coordinate²⁸. The energies of the low-lying (i.e. D_0 and D_1) states of the thiophenone cation have also been computed at selected geometries along the LIIC pathways (Fig. 3(a), dashed lines). In the Franck-Condon region, these states are characterized by removal of an electron from, respectively, the n(S) and n(O) lone pair orbitals. As Fig. 3(a) shows, the topographies of the various PESs of neutral thiophenone vary strongly along the LIIC pathways, but the energies of the D₀ and D₁ states of the cation show a smooth and very gradual increase. The energy differences (ΔE) between the D_1/D_0 and the S_2/S_1 potentials along the LIIC pathways (inset in Fig. 3(a)) increase dramatically from the FC point out to the S₁/S₀ MECI. The calculations allow assignment of the experimentally observed rapid increase in BE with increasing Δt to the ultrafast depopulation of the S₂ state and electronic deactivation to the S₀ state, resulting in highly vibrationally excited ground state molecules. We note that the calculated ΔE values are consistently slightly lower than the experimental BE values. Such underestimation of (experimental) IP values by (X)MS-CASPT2 methods is well-known³⁰ and, in the present case, can also be related to the choice of basis set (see Section 2.2 of the Supplementary Information).

The fates of the photoexcited thiophenone molecules were explored further by running trajectory surface hopping (TSH) calculations from the photo-prepared S_2 state at the SA(4)-CASSCF(10/8) level of theory. These results are detailed in Section 2 of the Supplementary Information, and only the main features of the dynamics are highlighted here. As expected from inspection of the LIIC pathways, the initial S_2 population rapidly decays to the S_1 state and population appears almost immediately on the S_0 PES as shown in Fig. 3(b). All population is transferred to the S_0 state within 350 fs of UV excitation. Figure 3(c) displays a swarm of 46 TSH trajectories that mimic the relaxation dynamics of the thiophenone wavepacket and demonstrate that the ultrafast deactivation from S_2 to S_1 to S_0 is driven by a ballistic ring-opening process. The trajectories start to spread after ~ 50 fs; most remain ring-opened upon becoming $S_0^{\#}$ molecules, but some re-adopt a (vibrationally hot) cyclic configuration.

The conclusions from the TSH calculations match well with the experimental time-resolved photoelectron yields for the BE ranges selected to span the predicted IP_{vert} values along the LIIC (Figs. 2(b) and 2(c)). The yield in the BE range corresponding to vertical ionization from the S_2 state (blue trace in fig. 2(b)) shows a narrow transient signal, the width of which is largely determined by the temporal instrument response function. With increasing Δt , this transient signal shifts to higher BE, broadens somewhat and gains a longer time tail (fig. 2(c)). Guided by the inset in Fig. 3(a), these observed changes are all consistent with the wavepacket evolving on the S_2 PES

(sampled most cleanly by intensities at BE \leq 5.5 eV), and subsequent non-adiabatic coupling with the S₁ state (which will be sampled most efficiently in the 6 \leq BE \leq 7 eV range), and thence with the S₀ PES (which will start to be sampled at BE \geq 7 eV). Ionization of S₀[#] molecules accounts for the tails in the transients for the higher energy BE slices in Fig. 2(c); the build-up of S₀[#] population (green crosses in Fig. 2(b)) plateaus at $\Delta t \geq$ 300 fs. These comparisons serve to reinforce the interpretation developed from considering the LIIC pathways (Fig. 3(a)) that the experimentally observed increase in BE is a signature of the ultrafast decay of thiophenone (S₂) molecules to high S₀[#] levels.

Ground-state dynamics and reaction products. One key feature of the present experimental study is that the response of UV-excited thiophenone molecules can be followed not just en route to, but also after reaching, the S₀ PES. Fig. 4(a) shows photoelectron spectra recorded at several pumpprobe delays in the range $10 \le \Delta t \le 600$ ps. Most of the photoelectron intensity of interest at these large Δt values lies in the range $8.0 \le BE \le 9.6$ eV, and the spectrum appears to consist of different contributions whose weights are Δt -dependent; the intensity of the feature at lower BE (peaking at BE \sim 8.8 eV) appears to increase relative to that of the feature peaking at BE \sim 9.3 eV. To simulate the ground state dynamics, the foregoing non-adiabatic molecular dynamics calculations using TSH in the lowest four electronic states were combined with ab initio molecular dynamics (AIMD, see Computational Details) on the S₀ PES. From an electronic structure perspective, this required switching from a SA-CASSCF description (used for the excited-state dynamics) to an unrestricted density functional theory (UDFT) picture using the PBE0 exchange/correlation functional; the SA-CASSCF active space employed for the TSH dynamics became unstable when the trajectories were prolonged on the S₀ PES, but AIMD with UDFT was found to offer a stable alternative and allowed long-time simulation of the $S_0^{\#}$ species (see, e.g. Ref. 31). Tests demonstrating the validity of this approach for the present system are reported in Supplementary Information Section 2.5.

To initiate the $S_0^{\#}$ molecular dynamics after passage through the S_1/S_0 seam of intersection, the AIMD trajectories were launched from the nuclear coordinates and with the momenta given by the TSH trajectories upon reaching the S_0 state. Thus the present AIMD simulations are not *per se* in a ground-state thermal equilibrium, since the internal energy of the molecule at the start of the S_0 -state dynamics calculation depends on the history of the TSH trajectory in the excited state, *i.e.* the approach allows description of non-statistical effects in the hot S_0 -state dynamics. In total, 22 AIMD trajectories were propagated until t = 2 ps and, to explore the longer time dynamics, 10 of these were propagated further to t = 100 ps (see Computational Details and Section 2.10 in the Supplementary Information). Since each is a continuation of an excited-state trajectory, the starting configuration in each case involves a ring-opened or highly stretched molecule.

The AIMD simulations reveal formation of several different photoproducts within the earliest timescales of these dynamics. Ring closure (resulting in re-formation of 'hot' thiophenone molecules) is observed, as is the formation of the acyclic isomers 2-thioxoethylketene (P1), 2-(2-sulfanylethyl)ketene (P2), and 2-(2-thiiranyl)ketene (P3) (see Fig. 4(b) for structures). Interconversion between these isomers was observed in most trajectories within 2 ps (see *e.g.* Supplementary Fig. 12). The histogram labelled 'other' in Fig. 4(b) includes all molecular geometries that could not be attributed to P1, P2, P3 or closed-ring thiophenone products. These

rare 'other' geometries often correspond to transient configurations in the act of interconverting between the dominant photoproducts and are mostly observed within 500 fs of accessing the S_0 -state PES. It is important to emphasize that these AIMD calculations (and the gas-phase experiments) involve isolated molecules. The potential energy acquired by thiophenone upon photoexcitation is converted, in part, to nuclear kinetic energy during the non-radiative decay to the S_0 state, but these are closed systems; no energy dissipation is possible and the resulting $S_0^{\#}$ species are highly energetic.

Experimentally, the BEs of the $S_0^{\#}$ species formed via non-radiative de-excitation are concentrated in a narrow (~1 eV, full width at half maximum (FWHM)) band centered at ~9 eV, as shown in Figs. 4(a) and 4(c). Yet the AIMD simulations indicate that this ensemble of $S_0^{\#}$ species must contain a range of structures with high internal energy. Thus the 22 AIMD outputs were analyzed further. Specifically, the molecular geometry was extracted every 10 fs from each AIMD trajectory, yielding a pool of >4000 geometries. These were grouped by photoproduct (see Section 2.6 in the Supplementary Information) and, for each geometry, the IP_{vert} value between the S₀ and D₀ states was calculated (using MP2-F12/cc-pVDZ-F12) to provide an estimate of the BE. As Fig. 4(b) shows, the histograms of the IP_{vert} values for each photoproduct span a narrow range, and the ground state photoproducts P1, P2 and P3 display similar distributions of vertical IPs. This reflects the fact that, in each case, ionization involves removal of an electron from an orbital with a high degree of n(S) character. The distribution associated with re-formed closed-ring thiophenone species is centered at slightly higher IPvert values. For completeness, we note that the predicted distribution of $S_0 \rightarrow D_0$ IP_{vert} values for thiophenone molecules without the extra kinetic energy induced by photoexcitation and subsequent relaxation (derived from AIMD simulations of thiophenone initiated with an internal energy equal to the zero-point energy only) is centered at yet higher IP_{vert}, is much narrower and, as Supplementary Fig. 15 shows, is in very good accord with the lowest energy peak in the measured He I photoelectron spectrum²⁹.

Returning to the 'hot' $S_0^\#$ molecules, the 22 AIMD outputs predict a narrow overall distribution of IP_{vert} values (Fig. 4(d)) that, as Fig. 4(c) shows, matches well with the TRPES data summed over the delay range $0.5 \le \Delta t \le 2$ ps. The 10 AIMD outputs propagated to t = 100 ps (see Supplementary Fig. 17) provide additional insights into the longer time dynamics of these $S_0^\#$ molecules. Analysis of the (admittedly small number of) long time trajectories reveal (i) irreversible conversion of closed-ring to open-ring isomers and (ii), in several cases, unimolecular decay of the $S_0^\#$ species to CO + thioacrolein (CH₂CHC(H)S) products. The first IP_{vert} of thioacrolein is 8.9 eV (see Ref. 32), a value reproduced computationally in the present work (see Section 2.10 in the Supplementary Information). Thus, recalling Fig. 4(b), we note that all closed-ring to open-ring transformations (including the fragmentation process) will cause a net transfer of $S_0^\#$ population to species with lower IP_{vert} (*i.e.* lower BE) values – consistent with the experimental observations (Fig. 4(a)).

Conclusions

A previous transient infrared absorption spectroscopy study of the UV photoexcitation of thiophenone in solution (*i.e.* in an environment where any product vibrational excitation is rapidly dissipated through interaction with the solvent) 18 demonstrated the formation of acyclic

photoproduct(s) with ketene structures and the recovery of (vibrationally cold) ground state thiophenone molecules. These earlier studies lacked the temporal resolution to probe the ring opening mechanism directly, and the only $S_0^\#$ dynamics amenable to investigation was vibrational relaxation via interaction with the solvent molecules. Such limitations are swept aside in the present study, wherein time-resolved XUV photoelectron spectroscopy studies of the isolated (gas phase) molecules at a seeded FEL, in combination with high-level *ab initio* theory, have allowed detailed visualization of the electronic and, particularly, the structural dynamics of this complex photo-induced ring-opening reaction, revealing the initial motion following photoexcitation, the non-adiabatic coupling to the S_0 PES as an open-ring biradical, and the subsequent isomerizations and eventual decay of the highly vibrationally excited S_0 -state species. The match between theory and experiment spans both the excited-state decay rates and the more challenging athermal rearrangements that occur after non-adiabatic coupling to the S_0 state and onwards to photoproducts.

The use of sufficiently high-energy probe photons is key to tracking the full decay dynamics, i.e. the ultrafast evolution of the photoexcited wavepacket to the S₀ state and the nuclear dynamics of the resulting highly vibrationally excited S₀ molecules. The increase in BE observed immediately post-photoexcitation is a signature of the ultrafast decay of the nuclear wavepacket from the S₂ state, via the S1 state, towards the electronic ground state, enabled by elongation and eventual scission of the S-CO bond. The evolving molecules couple to the S₀ PES with a range of geometries and nuclear momenta, which govern the subsequent athermal rearrangements of the $S_0^{\#}$ species. These vibrationally excited S_0 molecules are highly fluxional and can adopt at least three identified open-ring structures or re-form the parent thiophenone and have sufficient internal energy to dissociate (by loss of a CO moiety); the deduced ground state dynamics serve to bolster a recent prediction that isomerization of energized molecules prior to dissociation might well be the rule rather than the exception in many polyatomic unimolecular processes³³. The distribution of vertical IPs computed from the AIMD trajectories on the S₀ PES reproduces the narrow spread of BEs observed experimentally and can be traced to the localized nature of the sulfur lone pair orbital that is the dominant contributor to the highest occupied molecular orbital in each species. Distinguishing the various open-ring products by valence-shell photoelectron spectroscopy is challenging given their very similar first IPs. Ultrafast X-ray or electron diffraction studies might be able to address such structural challenges if sufficient scattering signal can be obtained despite the low sample vapor pressure.

References

- 1. Minitti, M.P. et al. Imaging Molecular Motion: Femtosecond X-Ray Scattering of the Ring Opening in 1,3- Cyclohexadiene. *Phys. Rev. Lett.* **114**, 255501 (2015).
- 2. Pullen, M. G. et al. Imaging an aligned polyatomic molecule with laser-induced electron diffraction. *Nature Communications* **6**, 7262 (2015).
- 3. Wolter, B. et al. Ultrafast electron diffraction imaging of bond breaking in di-ionized acetylene. *Science* **354**, 308–312 (2016).

- 4. Attar, A.R. et al. Femtosecond x-ray spectroscopy of an electrocyclic ring-opening reaction. *Science* **356**, 54–59 (2017).
- 5. Schuurman, M.S. & Stolow, A. Dynamics at Conical Intersections. *Annu. Rev. Phys. Chem.* **69**, 427–450 (2018).
- 6. Wolf, T.J.A. et al. The photochemical ring-opening of 1,3-cyclohexadiene imaged by ultrafast electron diffraction. *Nature Chemistry* **11**, 504–509 (2019).
- 7. Ruddock, J. M. et al. A deep UV trigger for ground-state ring-opening dynamics of 1,3-cyclohexadiene. *Science Advances* **5**, eaax6625 (2019).
- 8. Stankus, B. et al. Ultrafast X-ray scattering reveals vibrational coherence following Rydberg excitation. *Nature Chemistry* **11**, 716–721 (2019).
- 9. Browne, W. R. & Feringa, B. L. Light Switching of Molecules on Surfaces. *Annu. Rev. Phys. Chem.* **60**, 407–428 (2009).
- 10. Kumpulainen, T., Lang, B., Rosspeintner, A. & Vauthey, E. Ultrafast Elementary Photochemical Processes of Organic Molecules in Liquid Solution. *Chem. Rev.* **117**, 10826–10939 (2017).
- 11. Qi, J. et al. Light-driven transformable optical agent with adaptive functions for boosting cancer surgery outcomes. *Nature Communications* **9**, 1848 (2018).
- 12. Deb, S. & Weber, P. M. The Ultrafast Pathway of Photon-Induced Electrocyclic Ring-Opening Reactions: The Case of 1,3-Cyclohexadiene. *Annu. Rev. Phys. Chem.* **62**, 19–39 (2011).
- 13. Arruda, B.C. & Sension, R.J. Ultrafast polyene dynamics: the ring opening of 1,3-cyclohexadiene derivatives. *Phys. Chem. Chem. Phys.* **16**, 4439–4455 (2014).
- 14. Petrović, V. S. et al. Transient X-Ray Fragmentation: Probing a Prototypical Photoinduced Ring Opening. *Phys. Rev. Lett.* **108**, 253006 (2012).
- 15. Rudakov, F. & Weber, P. M. Ground State Recovery and Molecular Structure upon Ultrafast Transition through Conical Intersections in Cyclic Dienes. *Chem. Phys. Lett.* **470**, 187–190 (2009).
- 16. Adachi, S., Sato, M. & Suzuki, T. Direct Observation of Ground-State Product Formation in a 1,3-Cyclohexadiene Ring-Opening Reaction. *J. Phys. Chem. Lett.* **6**, 343–346 (2015).
- 17. Breda, S., Reva, I., Fausto, R. UV-induced unimolecular photochemistry of 2(5H)-furanone and 2(5H)-thiophenone isolated in low temperature inert matrices. *Vib. Spectrosc.* **50**, 57-67 (2009).
- 18. Murdock, D. et al. Transient UV pump–IR probe investigation of heterocyclic ringopening dynamics in the solution phase: the role played by nσ* states in the photoinduced reactions of thiophenone and furanone. *Phys. Chem. Chem. Phys.* **16**, 21271–21279 (2014).
- 19. Allaria, E. et al. Highly coherent and stable pulses from the FERMI seeded free-electron laser in the extreme ultraviolet. *Nature Photonics* **6**, 699–704 (2012).
- 20. Stolow, A., Bragg, A. E. & Neumark, D. M. Femtosecond Time-Resolved Photoelectron Spectroscopy. *Chem. Rev.* **104**, 1719–1757 (2004).

- 21. Suzuki, T. Time-resolved photoelectron spectroscopy of non-adiabatic electronic dynamics in gas and liquid phases. *Inter. Rev. Phys. Chem.* **31**, 265–318 (2012).
- 22. Iikubo, R., Sekikawa, T., Harabuchib, Y. & Taketsugubet, T. Structural dynamics of photochemical reactions probed by time-resolved photoelectron spectroscopy using high harmonic pulses. *Faraday Discussions* **194**, 147–160 (2016).
- 23. Nishitani, J., West, C.W., Higashimura, C. & Suzuki, T. Time-resolved photoelectron spectroscopy of polyatomic molecules using 42-nm vacuum ultraviolet laser based on high harmonics generation. *Chemical Physics Letters* **684**, 397–401 (2017).
- 24. Smith, A.D. et al. Mapping the Complete Reaction Path of a Complex Photochemical Reaction. *Phys. Rev. Lett.* **120**, 183003 (2018).
- 25. von Conta, A. et al. Conical-intersection dynamics and ground-state chemistry probed by extreme-ultraviolet time-resolved photoelectron spectroscopy. *Nature Communications* **9**, 3162 (2018).
- 26. Squibb, R.J. et al. Acetylacetone photodynamics at a seeded free-electron laser. *Nature Communications* **9**, 63 (2018).
- 27. Gorobtsov, O. Y., et al., Seeded X-ray free-electron laser generating radiation with laser statistical properties, *Nature Communications* **9**, 4498 (2018).
- 28. Xie, B.-B. & Fang, W.-H. Combined Quantum Trajectory Mean-Field and Molecular Mechanical (QTMF/MM) Nonadiabatic Dynamics Simulations on the Photoinduced Ring-Opening Reaction of 2(5H)-Thiophenone. *ChemPhotoChem* **3**, 897–906 (2019).
- 29. Chin, W.S. et al. He I and He II photoelectron spectra of thiophenones. *J. Electron Spectroscopy Related Phenomena* **88–91**, 97–101 (1998).
- 30. Tao, H. et al. Ultrafast internal conversion in ethylene. I. The excited state lifetime. *J. Chem. Phys.* **134**, 244306 (2011).
- 31. Mignolet, B., Curchod, B. F. E. & Martinez, T. J. Rich Athermal Ground-State Chemistry Triggered by Dynamics through a Conical Intersection. *Angew. Chem., Int. Ed.* **55**, 14993–14996 (2016).
- 32. Bock, H., Mohmand, S., Hirabayashi, T. & Semkow, A. Gas-phase reactions. 29. Thioacrolein. *J. Am. Chem. Soc.* **104**, 312-313 (1982).
- 33. Yang, C.-S., Bhattacharyya, S., Liu, L., Fang, W.-h. & Liu, K. Real-time tracking of the entangled pathways in the multichannel photodissociation of acetaldehyde. *Chem. Sci.* DOI: 10.1039/d0sc00063a

Acknowledgements

S.P., J.T., and D.R. were supported by the National Science Foundation (NSF) grant PHYS-1753324. S.P. was also partially supported by the Chemical Sciences, Geosciences, and Biosciences Division, Office of Basic Energy Sciences, Office of Science, U.S. Department of Energy (DOE) under Grant No. DE-FG02-86ER13491. Travel to FERMI for S.P., D.M.P.H., R.M., J.T., and D.R. was supported by LaserLab Europe. This work made use of the facilities of the Hamilton HPC Service of Durham University. M.N.R.A., C.S.H. and R.A.I. are grateful to the Engineering and Physical Sciences Research Council (EPSRC) for funding (EP/L005913/1), while L.M.I. acknowledges the EPSRC for a Doctoral Studentship (EP/R513039/1). C.S.H. also

acknowledges funding from the Australian Research Council (ARC, DE200100549). M.N.R.A. is grateful to Prof W.-H. Fang (Beijing Normal University) for permission to share data from Ref. 28 prior to its publication. B.F.E.C. acknowledges funding from the European Union Horizon 2020 research and innovation programme under grant agreement No 803718 (SINDAM). D.M.P.H. was supported by the Science and Technology Facilities Council, UK. R.F. and R.J.S. acknowledge financial support from the Swedish Research Council, the Knut and Alice Wallenberg Foundation, Sweden, and the Faculty of Natural Science of the University of Gothenburg. We thank the technical and scientific teams at FERMI for their hospitality and their support during the beamtime. We also acknowledge helpful discussions with Artem Rudenko during the preparation of the beamtime proposal and during the data interpretation and with Surjendu Bhattacharyya during the data analysis and interpretation.

Author Contributions

R.B., R.A.I., C.S.H., M.N.R.A. and D.R. conceived the experiment, the plans for which benefitted from further input from R.Fo., D.M.P.H. and A.R.. S.P., R.A.I., R.B., C.C., A.D., B.E., R.Fe., M.D.F., L.G., C.S.H., D.M.P.H., R.M., O.P., K.C.P., A.R., R.J.S., J.T., M.N.R.A. and D.R. conducted the experiment at the FERMI free-electron laser facility. The magnetic bottle spectrometer was provided and operated by R.Fe. and R.J.S.. C.C., M.D.F. and O.P. prepared and operated the beamline and the Low Density Matter (LDM) instrument. A.D. and L.G. prepared and operated the optical laser and the free-electron laser, respectively. L.M.I. and B.F.E.C. performed the *ab initio* simulations with contributions from R.A.I.. S.P. and J.T. analyzed the experimental data with contributions from R.Fo., C.S.H., R.A.I., R.M. and A.R.. S.P., L.M.I., R.B., R.Fo., M.N.R.A., B.F.E.C. and D.R. interpreted the results and wrote the manuscript with input from all the authors.

Competing interests

The authors declare no competing interests.

Figure Legends

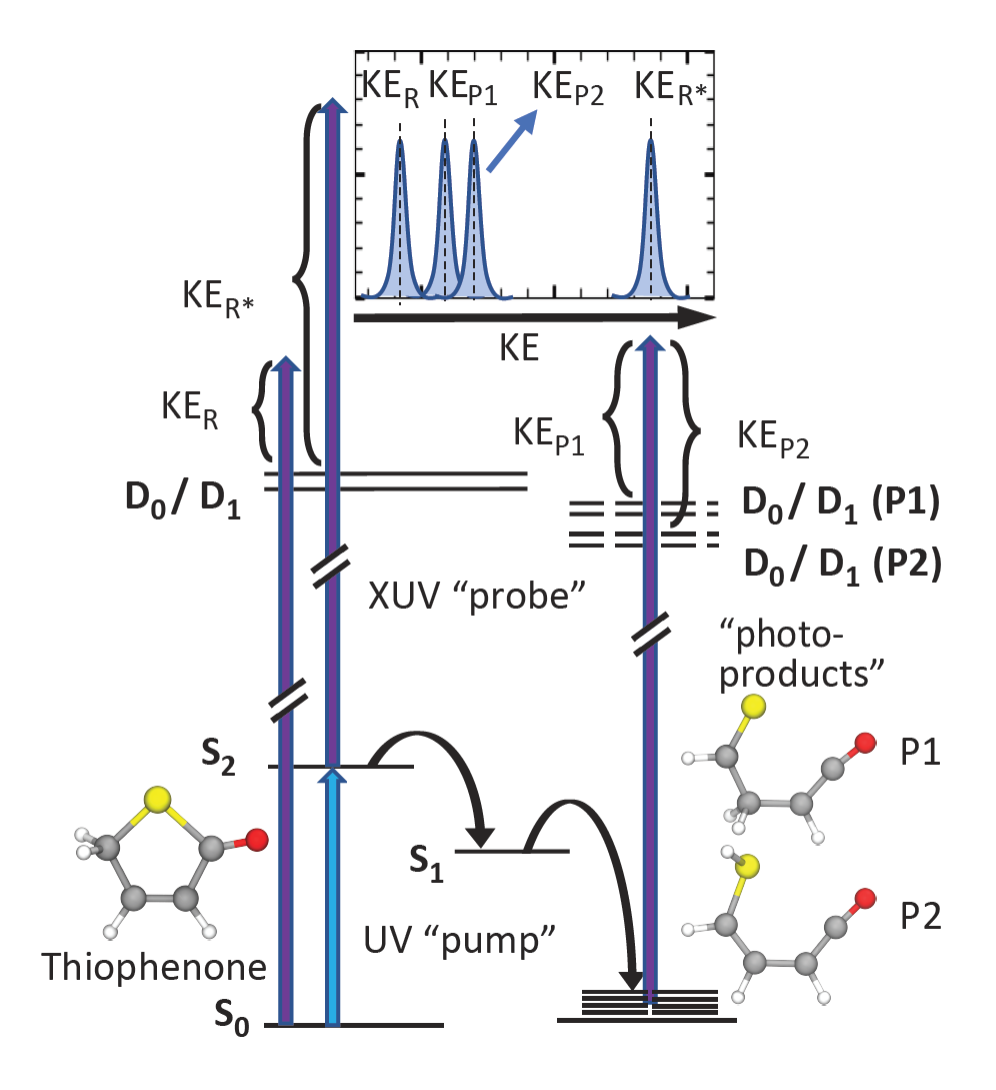


Figure 1: Schematic of the UV excitation, ring opening and photoionization of thiophenone. The molecule is photoexcited from its ring-closed ground state (S_0) to an electronically excited state (S_2) . It evolves through an optically dark excited state (S_1) back to the (vibrationally excited) S_0 state of several possible reaction products (P1, P2, etc.). The XUV probe photon energy is sufficient to ionize thiophenone and all reaction products from both ground and excited states into several ionic final states $(D_0, D_1, etc.)$. The time-evolving electron kinetic energy (KE) spectrum (top) thus consists of contributions from the ground and excited states of thiophenone (denoted as R and R*, respectively) and from the different products. In the depictions of the molecular geometry, carbon atoms are shown in grey, hydrogen in white, oxygen in red, and sulfur in yellow.

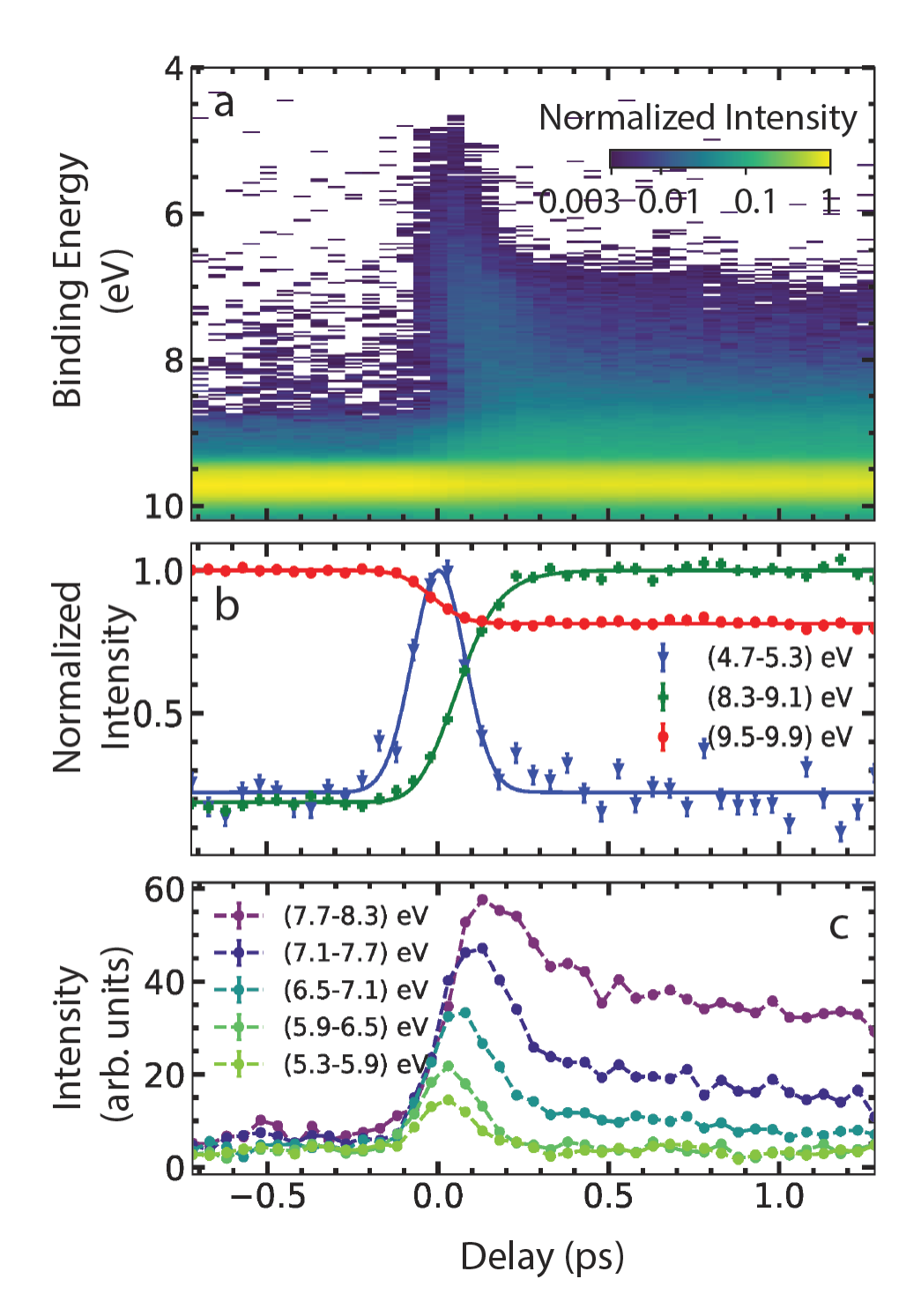


Figure 2: Time-dependent photoelectron spectra of UV-excited thiophenone. (a) Measured photoelectron yield as a function of binding energy (BE) and time delay (Δt) between pump and probe pulses (see Supplementary Fig. 2 for a plot over a wider range of signal intensities, binding energies and delays). Negative Δt corresponds to the FEL pulse preceding the UV pulse, positive Δt to the UV pulse preceding the FEL pulse, while the color represents the photoelectron yield. Regions with an intensity below ~ 0.003 are shown in white. Delay-dependent photoelectron yields

for (b) three BE ranges selected to illustrate the photoinduced de-population of the S_0 state (red circles), population of the S_2 state (blue triangles), and the build-up of vibrationally excited $S_0^\#$ photoproducts (green crosses); and (c) five contiguous 0.6 eV-wide BE slices that inform on the evolution from photoexcited S_2 to internally excited $S_0^\#$ molecules. Statistical error bars are included but are generally smaller than the symbol size. The parameters of the least-square fits shown as solid lines in (b) are summarized in Supplementary Table 1, while the dashed lines in (c) just join the dots for better visibility. The data in (b) have been normalized such that the maximum value of the fit is at 1 for each curve, whereas the data in (c) are displayed on a common intensity scale.

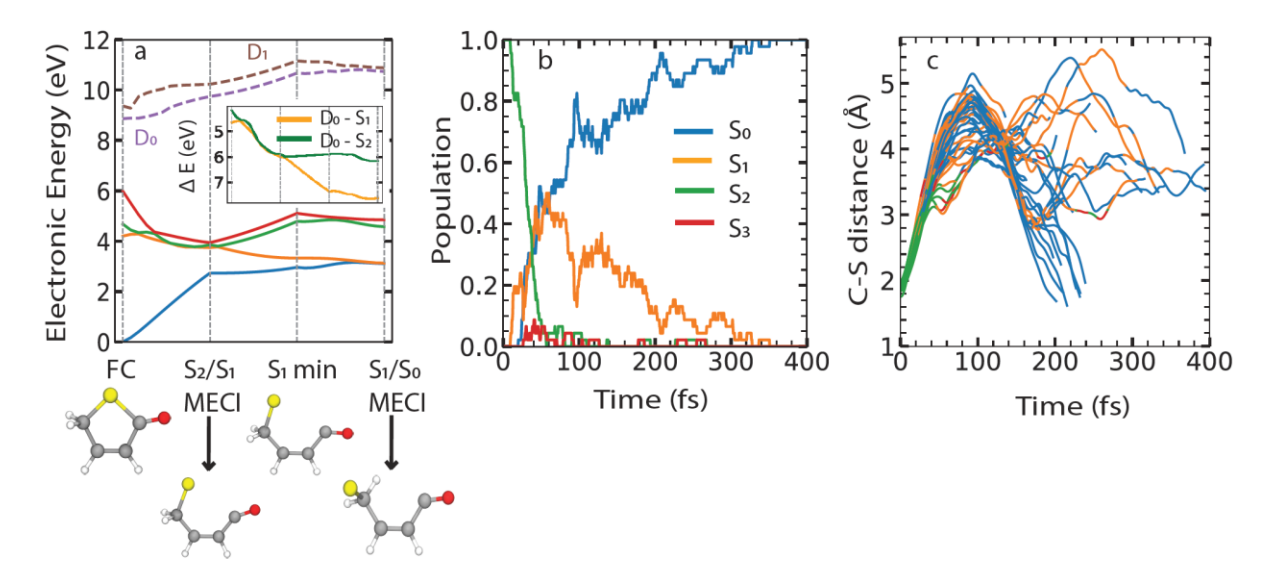


Figure 3: Ab initio calculations of potential energy surfaces and excited-state dynamics. (a) PESs for the lowest neutral singlet (solid lines) and cationic doublet (dashed lines) electronic states of thiophenone along linear interpolation in internal coordinates (LIIC) pathways between different critical geometries. Electronic energies were obtained using XMS(4)-CASPT2(10/8) for the neutral and XMS(4)/CASPT2(9/8) for the cationic form of thiophenone. The critical geometries, minima, and minimum energy conical intersections (MECIs), located using the SA(4)-CASSCF(10/8) level of theory, are indicated with light grey vertical lines, and the geometries of these critical points on the PESs of neutral thiophenone are shown below. LIIC pathways have then been computed between each critical point. The inset shows the electronic energy gap ΔE between the D₀ state of the cation and the second (S₂) or first (S₁) singlet states of neutral thiophenone for each point along the LIIC pathway. (b) Time-dependence of the S₃, S₂, S₁ and S₀ state populations provided by the TSH dynamics (46 trajectories). (c) Time-evolution of the C-S bond distance for each of these 46 trajectories, illustrating the prompt initial bond extension in all cases and the trajectory-dependent evolution from S₂ through S₁ to the S₀ state (coded in the same color as the PESs in (a) and (b)). The TSH trajectories were propagated until they experienced electronic structure instabilities in the ground state (see text).

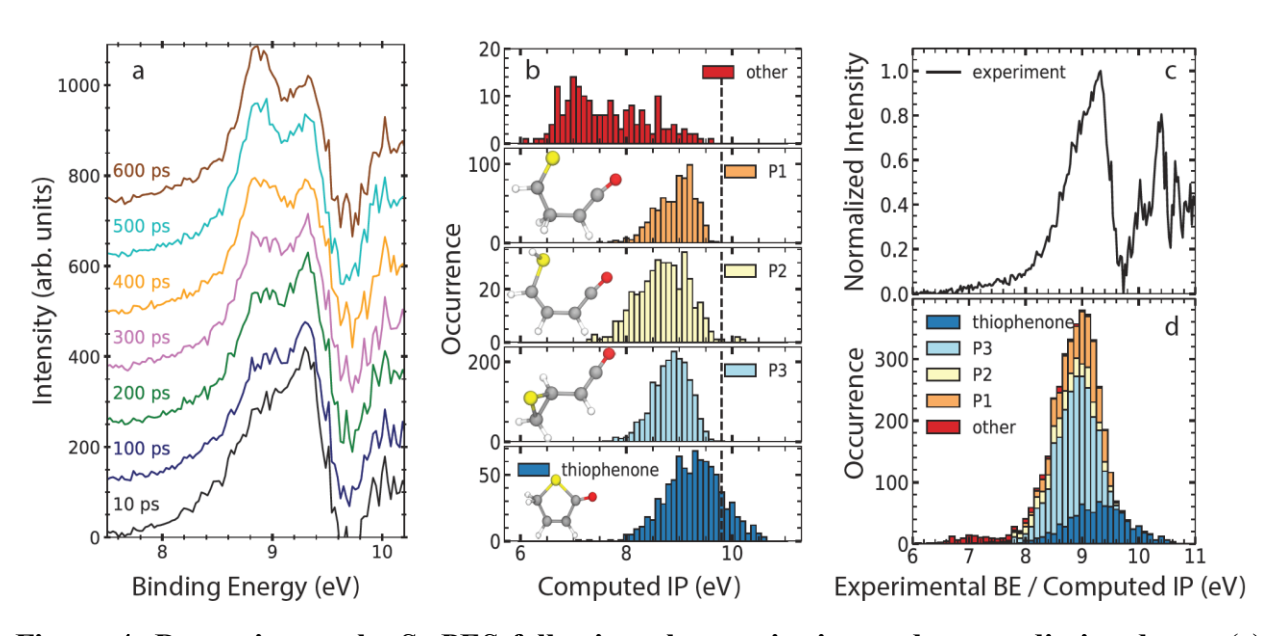


Figure 4: Dynamics on the S₀ PES following photoexcitation and non-radiative decay. (a) Photoelectron spectra for different pump-probe delays after subtraction of the signal from 'unpumped' thiophenone (S₀) molecules (see Supplementary Fig. 3 for details). The spectra are offset vertically for better visibility. (b) Histograms showing the number of occurrences of the various S₀ \rightarrow D₀ IP_{vert} values computed (at the MP2/cc-pVDZ-F12 level of theory) every 10 fs (for a total of 2 ps) along each AIMD trajectory on the S₀ PES, grouped by similarity to the molecular geometries identified as 2-thioxoethylketene (P1), 2-(2-sulfanylethyl)ketene (P2), 2-(2-thiiranyl)ketene (P3), and closed-ring thiophenone, along with a further small group labelled 'other' associated with internally hot molecules that are in the act of converting between stable isomeric forms at the time the trajectory was sampled (see text). The calculated IP_{vert} for thiophenone at its optimized ground-state geometry is indicated by a dashed vertical black line. (c) Experimental (subtracted) photoelectron spectrum summed over the delay range $0.5 \le \Delta t \le 2$ ps; the contribution at BE >9.8 eV is due to ionization of S₀[#] molecules to excited cationic states, which are not included in the present calculations (see also Supplementary Figs. 2, 3, and 15). (d) Sum of the five distributions of IP_{vert} values shown in panel (b).

Methods

Experimental: The experiment was performed at the low-density matter (LDM) beamline^{34,35} at the FERMI free-electron laser facility¹⁹. The FEL was operated at a photon energy of 19.24 eV, corresponding to the fourth harmonic of the seed laser, with an estimated pulse duration of 80 fs (FWHM)³⁶. The UV pump pulses with a center wavelength of 264.75 nm and 1.2 nm bandwidth were generated as the third harmonic of a Ti:Sapphire laser. Details relating to gas sample delivery, other laser pulse parameters (energies, durations and spot sizes) and tests to ensure that the reported effects scale linearly with pump and probe pulse parameters are reported in Section 1 of the Supplementary Information. A magnetic bottle type spectrometer^{26,37} (see Supplementary Fig. 1) was used to detect photoelectrons with high collection efficiency. A retardation voltage of 8 V was used to increase the resolution in the photoelectron range of interest (the approximate kinetic

energy resolution is $\delta E/E \approx 0.03$, with E being the final kinetic energy after retardation), cutting the photoelectron spectrum for binding energies of approximately 11 eV and above, as shown in Supplementary Fig. 2.

Data Acquisition and Analysis: Time-of-flight traces were recorded shot-by-shot while scanning the delay between the pump and probe pulses. The data shown in Fig. 1(a) consist of \sim 1650 shots per 50-fs delay bin. The single-shot spectra were normalized with respect to the FEL intensity (measured shot-to-shot³⁸) and then averaged for each delay bin. The electron time-of-flight was converted into photoelectron kinetic energy by calibrating the spectrometer using photoelectrons from the single-photon single ionization of helium at multiple harmonics, *i.e.*, different photon energies, of the FEL. The photoelectron energies were then converted to binding energy by subtracting the photoelectron energy from the FEL photon energy.

Computational Details:

Critical points and linear interpolation in internal coordinates

Critical points of the thiophenone PESs – S₀ minimum, S₁ minima, S₂/S₁ and S₁/S₀ minimum energy conical intersections (MECIs) – were located using SA(4)-CASSCF(10/8)^{39,40} and a 6-31G* basis set^{41,42} as implemented in Molpro 2012⁴³. Pathways connecting these different critical points of the PESs were produced by linear interpolations in internal coordinates (LIICs)⁴⁴. Some of the advantages and limitations of LIICs are summarized in Section 2.2 in the Supplementary Information. Electronic energies for thiophenone were computed along the LIIC pathways at the SA(4)-CASSCF(10/8) and XMS(4)-CASPT2(10/8)^{45,46} levels of theory using, in all cases, a 6-31G* basis set (see Supplementary Figs. 7 and 8). The electronic energies for the thiophenone cation were also computed along the LIICs using SA(4)-CASSCF(9/8) and XMS(4)-CASPT2(9/8). All XMS-CASPT2 calculations were performed with the BAGEL software⁴⁷, employing the corresponding SA-CASSCF wavefunction from Molpro 2012 as a starting point. A level shift⁴⁸ of 0.3 E_h was used in all XMS-CASPT2 calculations to prevent the appearance of intruder states. For details on the calculations of ionization potentials, including benchmarking studies justifying this choice of basis set, see Section 2 in the Supplementary Information.

Trajectory surface hopping dynamics

The excited-state dynamics of thiophenone following photoexcitation were simulated using the mixed quantum/classical dynamics trajectory surface hopping (TSH) method, employing the fewest-switches algorithm⁴⁹. All details regarding these dynamics are provided in Section 2 of the Supplementary Information.

Ab initio molecular dynamics to t = 2 ps and t = 100 ps

Ab Initio Molecular Dynamics (AIMD) calculations of the photoproducts formed during the TSH dynamics were conducted on the S₀-state PES using unrestricted DFT with the PBE0 exchange/correlation functional⁵⁰ and a 6-31G* basis set, employing the GPU-accelerated software TeraChem⁵¹. The initial conditions (nuclear coordinates and velocities) for each AIMD trajectory (22 in total, drawn randomly from the pool of TSH trajectories) were extracted from the TSH dynamics when the trajectory reached the S₀ state. At this initial point of configuration space, the SA-CASSCF wavefunction already exhibits a dominant closed-shell character (confirmed at the XMS-CASPT2 level of theory, see Section 2.5 in the Supplementary Information for additional

details). A small (0.1 fs) time step was used to ensure proper total energy conservation for all trajectories, and the length of each (constant total energy) trajectory was set such that the total TSH+AIMD dynamics extend to 2 ps. This strategy necessarily restricts the dynamics to the S_0 PES; the legitimacy of this procedure was validated by test trajectories on S_0 , which show the energy separation between the ground and excited electronic states increasing rapidly upon leaving the region of the S_1/S_0 seam of intersection. To explore the long-time dynamics of the different photoproducts, 10 of the 22 trajectories were propagated further, to t = 100 ps, using the same methodology except for a slightly longer time step of 0.25 fs.

Analysis of the 2-ps AIMD and vertical ionization energy distribution

The 22 AIMD trajectories propagated until t = 2 ps were used to analyze the distribution of IP_{vert} values for the $S_0^\#$ photoproducts. For each AIMD trajectory, molecular geometries were sampled every 10 fs, leading to a pool of >4000 S_0 molecular configurations. Each configuration was assigned to one of the possible photoproducts identified in Ref. 18 based on characteristic atomic connectivities determined by measuring bond lengths or angles (see Supplementary Fig. 13). If such assignment was not possible, the configuration was given the label 'others'. These were often due to a transient configuration between two photoproducts. The IP_{vert} of each configuration was then computed at the MP2-F12/cc-pVDZ-F12 level of theory (this level of theory was benchmarked against CCSD(T)-F12/cc-pVDZ-F12, see Section 2.8 in the Supplementary Information). The resulting distribution of $S_0 \rightarrow D_0$ IP_{vert} values provides an approximation of the low-energy part of the experimental BE spectra. The same methodology, applied to ground-state dynamics of 'cold' thiophenone, successfully reproduces the first peak in the experimental He I photoelectron spectrum (see Supplementary Fig. 15). All calculations were performed with Molpro 2012.

References (for Methods section)

- 34. Svetina, C. et al. The Low Density Matter (LDM) beamline at FERMI: optical layout and first commissioning. *J. Synchrotron Rad.* **22**, 538–543 (2015).
- 35. Lyamayev, V. et al. A modular end-station for atomic, molecular, and cluster science at the low density matter beamline of FERMI@Elettra. *J. Phys. B: At. Mol. Opt. Phys.* **46**, 164007 (2013).
- 36. Finetti, P. et al. Pulse Duration of Seeded Free-Electron Lasers. *Phys. Rev. X* 7, 021043 (2017).
- 37. Eland, J. H. D. et al. Complete two-electron spectra in double photoionization: the rare gases Ar, Kr, and Xe. *Phys. Rev. Lett.* **90**, 053003 (2003).
- 38. Zangrando, M. et al. Recent results of PADReS, the Photon Analysis Delivery and REduction System, from the FERMI FEL commissioning and user operations. *J. Synchrotron Rad.* **22**, 565–570 (2015).
- 39. Werner, H.-J. Matrix-formulated direct multiconfiguration self-consistent field and multiconfiguration reference configuration-interaction methods. *Advances in Chemical Physics: Ab Initio Methods in Quantum Chemistry Part 2* **69**, 1–62 (1987).

- 40. Roos, B. O. The complete active space self-consistent field method and its applications in electronic structure calculations. *Advances in Chemical Physics: Ab Initio Methods in Quantum Chemistry Part 2* **69**, 399–445 (1987).
- 41. Hehre, W. J., Ditchfield, R. & Pople, J. A. Self-Consistent Molecular Orbital Methods. XII. Further extensions of Gaussian-type basis sets for use in molecular-orbital studies of organic-molecules. *J. Chem. Phys.* **56**, 2257- 2261(1972).
- 42. Hariharan, P. C. & Pople, J. A. Influence of polarization functions on molecular-orbital hydrogenation energies. *Theor. Chem. Acc.* **28**, 213–22 (1973).
- 43. Werner, H.-J. et al. MOLPRO, version 2012.1, a package of *ab initio* programs (http://www.molpro.net) (2012).
- 44. Hudock, H. R. et al. Ab initio molecular dynamics and time-resolved photoelectron spectroscopy of electronically excited uracil and thymine. *The Journal of Physical Chemistry A* **111**, 8500–8508 (2007).
- 45. Shiozaki, T., Győrffyet W., Celani, C. & Werner, H.-J. Communication: Extended Multi-State Complete Active Space Second-Order Perturbation Theory: Energy and Nuclear Gradients. *J. Chem. Phys.* **135**, 081106 (2011).
- 46. Granovsky, A. Extended Multi-Configuration Quasi- Degenerate Perturbation Theory: The New Approach to Multi-State Multi-Reference Perturbation Theory. *J. Chem. Phys.* **134**, 214113 (2011).
- 47. BAGEL Brilliantly Advanced General Electronic-structure Library, http://www.nubakery.org under the GNU General Public License
- 48. Ghigo, G., Roos, B. O & Malmqvist, P.A. A modified definition of the zeroth-order Hamiltonian in multiconfigurational perturbation theory (CASPT2). *Chem. Phys. Lett.* **396**, 142-149 (2004).
- 49. Tully, J.C. Molecular dynamics with electronic transitions. *J. Chem. Phys.* **93**, 1061–1071 (1990).
- 50. Adamo, C. & Barone, V. Toward reliable density functional methods without adjustable parameters: The PBE0 model. *J. Chem. Phys.* **110**, 6158–69 (1999).
- 51. Ufimtsev, I.S. & Martinez, T. J. Quantum Chemistry on Graphical Processing Units. 3. Analytical Energy Gradients, Geometry Optimization, and First Principles Molecular Dynamics. *J. Chem. Theory Comput.* **5**, 2619–2628 (2009).

Data availability

The data that support the findings of this study are available from the corresponding authors upon reasonable request.

Code availability

The analysis codes used to generate the data presented in this study are available from the corresponding authors upon reasonable request.